Research article

Xinping Zhang*

Plasmon extinguishment by bandedge shift identified as a second-order spectroscopic differentiation

https://doi.org/10.1515/nanoph-2020-0603
Received November 7, 2020; accepted January 20, 2021;
published online February 2, 2021

Abstract: Optical excitation of metallic nanostructures induces strong intraband transitions, leaving transient depletion below the Fermi level, which allows transient interband transition to this depletion band. This is equivalent to the lowering of the threshold for interband transitions and pushes the plasmonic band to the red. As a result, localized surface plasmon resonance (LSPR) is "extinguished" or "quenched" around the bandedge, in contrast, the interband optical absorption becomes enhanced and redshifted. The corresponding transient absorption (TA) signals have equal lifetimes and opposite signs. Moreover, the TA spectrum is found to be a second-order differential of the steady-state optical extinction spectrum over the studied band. This is a commonly existing mechanism for metallic nanostructures and verified with gold in this work. Such a discovery is completely different from the optical-excitation-induced redshift of LSPR through enhanced electronic scattering and is important for understanding the ultrafast spectroscopic response of plasmonic nanostructures with clear photophysical insights, supplying solid basis for exploring optical logic device and optical data processing techniques.

Keywords: bandedge shift; interband transition; intraband excitation; plasmon extinguishment; second-order differentiation; transient depletion.

1 Introduction

Optical excitation of metallic nanostructures may induce multifold electronic processes. Inter- and intraband transitions, plasmonic electron oscillation, and electron-phonon interactions are the principal processes [1, 2]. These interactions are responsible for the commonly observed ultrafast spectroscopic response of the plasmonic devices. Optical switch [3–6], optical logic circuits [7–10], metal-semiconductor hybrid devices [11, 12], and particle-on-film nanocavities [13] based on plasmonic nanostructures have been developed with promising characteristics for various applications. However, due to the complexity of the involved ultrafast optical processes, it is still a challenge to decompose the overlapped electronic interaction processes, which influences the precise understanding of the true physics and consequently limits the design and development of advanced optoelectronic devices. In particular, localized surface plasmon resonance is modulated by interband transitions [14–17]. Nevertheless, in most cases observations have been explained mainly by processes related to plasmonic electrons as general mechanisms. Although the transient spectroscopic response of plasmonic nanostructures has been widely investigated, electron–electron and electron–phonon scattering processes and the resultant redshift of localized surface plasmon resonance (LSPR) have been assigned as the main mechanisms to explain the photoelectronic processes. Such mechanisms explain very well the redshift of LSPR under optical excitation, which is observed roughly as a "first-order differential" [5] of the resonance spectrum, but they cannot explain the extensively observed transient spectroscopic response on the boundary between interband transitions and plasmonic resonance.

In this work, it is revealed that the most important optical response of the gold nanoparticles under femtosecond optical pulse excitation is the quenching of localized surface plasmon resonance and simultaneous enhancement of interband electronic transition, which

***Corresponding author: Xinping Zhang**, Institute of Information Photonics Technology, Faculty of Science, Beijing University of Technology, Beijing 100124, China,
E-mail: zhangxinping@bjut.edu.cn. https://orcid.org/0000-0001-6534-0004

results from the bandedge shift on the boundary between the interband and plasmon-band electronic processes. Moreover, the ultrafast spectroscopic response reveals an interesting mathematical operation on the optical extinction spectrum of the gold nanoparticles, which is a nearly precise "second-order differentiation". What is discovered here is the redshift of the interband-transition threshold and the resulted quenched LSPR on the band edge, which has not been discovered and described explicitly and definitely so far. In particular, the "second-order differential" is a fingerprint of the discovered mechanism. Such a mechanism applies to various nanostructures of different metallic materials at optical excitations strong enough to induce transient depletion within the conduction band.

2 Photophysical mechanisms

Figure 1 illustrates the basic mechanisms for the intraband excitation induced bandedge shift and the consequent quenching of the LSPR band. Before strong optical excitation, optical absorption is a result of interband transition, e.g. from 5*d* band to 6*sp* hybrid bands for gold, as shown in the left panel of Figure 1(a). The threshold for such a transition is generally observed at about 2.48 eV (or about 500 nm) for gold. Upon strong optical excitation, e.g. by femtosecond laser pulses, intraband transition (upward red arrow in Figure 1(a)) may lead to the depletion of the conduction band below the Fermi level, so that interband transitions are allowed to the conduction band below the Fermi level, as shown in the right panel of Figure 1(a). This is equivalent to the lowering of the threshold for interband transitions or shifting of the bandedge to the red. Thus, the band structure of the metallic nanostructures is modulated transiently, as shown in Figure 1(b). Due to the bandedge shift, interband transition is allowed at lower photon energy, so that the original boundary between interband transition (①) and plasmonic electron oscillation (③) processes becomes enhanced optical absorption (②). Such a bandshift also pushes the LSPR band to the red, leaving a quenched LSPR spectrum at the lower edge of the plasmon band (④). Consequently, two most important features can be observed in the transient absorption (TA) spectroscopic characterization: the positive TA at the enhanced interband transitions ② and the negative TA at the quenched LSPR ④, as illustrated in the plot of $\Delta A(\lambda)$ in Figure 1(c).

The optical extinction spectrum varying with wavelength (λ) before optical excitation (blue curve in Figure 1(b)) can be defined as $A(\lambda)$ with $A'(\lambda_0) = 0$, where function $A'(\lambda) = dA(\lambda)/d\lambda$ is a first-order differential of $A(\lambda)$ and λ_0 can be taken as the threshold wavelength for interband transitions. Redshift of the threshold wavelength

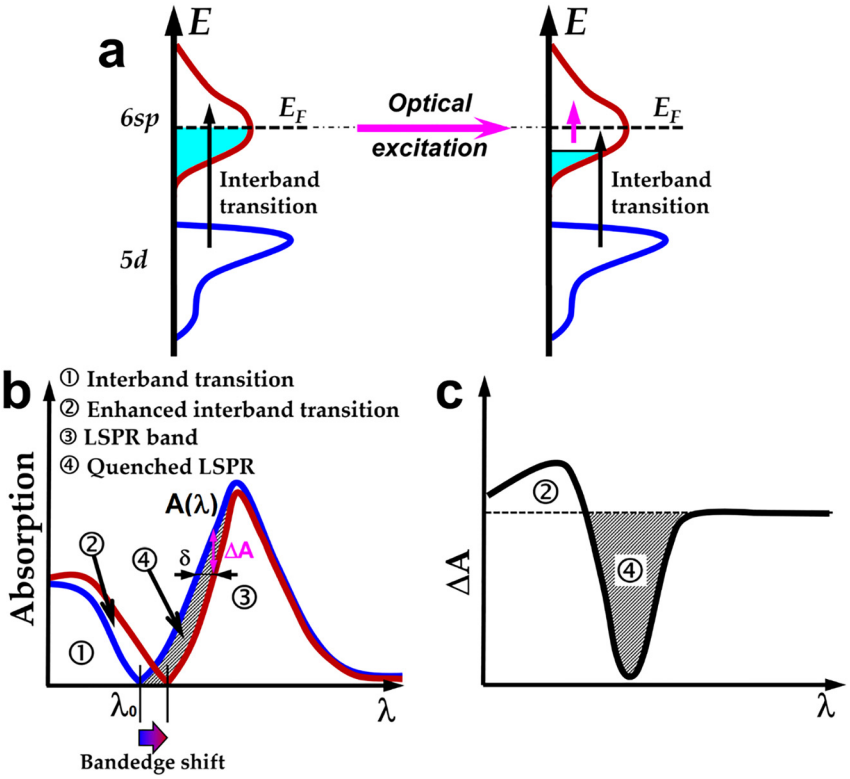

Figure 1: (a) Intraband optical excitation induced depletion of the conduction band below the Fermi level. (b) Redshift of the band edges due to the intraband depletion. (c) Bandedge shift induced enhanced interband transition (②) and quenched plasmonic optical extinction (④).

corresponds to an extension of the falling bandedge and shrinking of the rising edge, as shown by the red curve with respect to the blue in Figure 1(b). Clearly, the bandedge shift δ is a function of both λ and $A'(\lambda)$. It needs to be noted that even at strong optical excitation, the spectral shift of $\delta(\lambda)$ is quite small. What is measured in the TA spectroscopy is the value of $\Delta A(\lambda)$, which may be derived as:

$$\Delta A(\lambda) = A(\lambda + \delta(\lambda)) - A(\lambda) \approx A'(\lambda)\delta(\lambda) + A''(\lambda)\delta^2(\lambda)/2, \quad (1)$$

which is obtained by the expansion of function $A(\lambda + \delta(\lambda))$ at λ with a small change of δ with $A''(\lambda) = d^2A(\lambda)/d\lambda^2$. However, the function $A(\lambda)$ has a minimum and maximum at λ_0 and λ_1, respectively. Namely, we have $A'(\lambda_0) = A'(\lambda_1) = 0$. These two spectral locations actually locked the band structure of the quenched LSPR and the extended interband transitions. Therefore, around λ_0 and λ_1, we have:

$$\Delta A(\lambda) \approx A''(\lambda)\delta^2(\lambda)/2 \propto \cdot A''(\lambda), \quad (2)$$

where we assume small δ with much slower variation than $A''(\lambda)$. The assumption is reasonable with the system, since $|\delta| < \lambda_1 - \lambda_0$ is a very small change over the whole studied band.

Therefore, it can be understood that the TA spectrum ($\Delta A(\lambda)$) displays second-order differential ($A''(\lambda)$) features of the steady-state optical extinction spectrum of the metallic nanostructures. This is a unique feature for the bandedges on the boundary between interband transitions and the plasmon band. In turn, the second-order differential performance of the TA spectrum can be taken as an identity of the bandedge shift effect for explaining and recognizing the plasmonic quenching behavior. The experimental results in the following sections will prove that the spectrum in Figure 1(c) is almost an exact second-order differential of the intrinsic optical extinction spectrum (blue curve in Figure 1(b)), verifying the proposed photophysics.

3 Results and discussions

In the experiments, randomly distributed gold nanoparticles (AuNPs) with randomly distributed sizes on a planar glass substrate were chosen for the investigation, so that no other photonic resonance mode may disturb the spectroscopic response, as generally observed in periodic structures. The insets of Figure 2 show the scanning electron microscope (SEM) images of three different AuNP samples, where sample *A* consists of relatively larger particles with a lower density than *B*; sample *C* consists of round-shaped AuNPs with a large size distribution range but a lowest density, as compared with *A* and *B*; sample *B* has the smallest particle sizes but the highest distribution density. The measured optical extinction spectra on these samples *A*, *B*, and *C* are plotted in Figure 2 by the blue, black and red curves. All of these samples have been prepared by spin-coating colloidal gold nanoparticles with a diameter of 5–10 nm in toluene with a concentration of 100 mg/mL onto glass substrates before annealing at different temperatures. For sample *A* and *B*, an annealing temperature of 400 and 250 °C has been used, respectively. For sample *C*, an intermediate layer of S1805 photoresist is spin-coated onto the glass substrate before spin-coating the colloidal gold nanoparticles and an annealing at 500 °C is carried out to melt the gold and to remove the photoresist. After the annealing process, no photoresist remains on the substrate anymore, so that the resultant gold nanoparticles are sitting on a glass substrate without any other environmental medium. Thus, all samples simply consist of AuNPs on pure glass substrates, although they have different shapes, sizes, and distribution densities.

According to Figure 2, sample *A* exhibits strongest optical extinction with a largest spectral bandwidth (~113 nm) at FWHM and sample *C* has a smallest amplitude in optical extinction and a narrowest bandwidth (~81 nm). The optical extinction spectra of samples *A* and *B* are both peaked at about 562 nm, however, sample *C* has an optical extinction peak at about 553 nm. These performances are based on different distributions in shapes, sizes, homogeneities, and densities of the three samples. In the measurement of optical extinction spectra, a halide

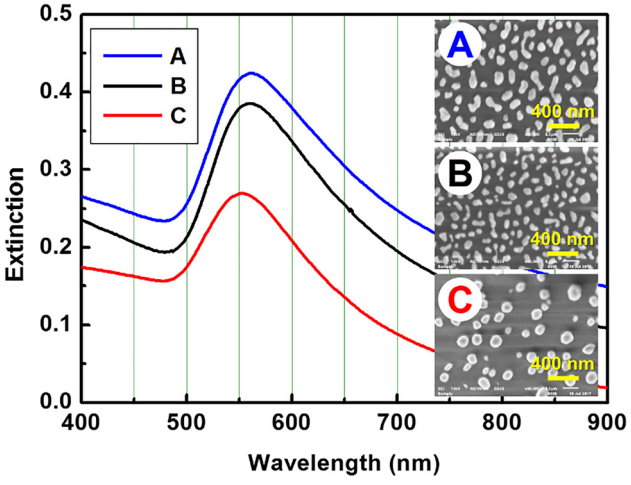

Figure 2: Optical extinction spectra measured on AuNP samples *A*, *B*, and *C*. The scanning electron microscope (SEM) images of *A*, *B*, and *C* are presented in the inset.

tungsten lamp was used to supply the broad-band white-light source and a USB4000 spectrometer from Ocean Optics was used to detect the transmission spectra through the samples. The optical extinction spectra were calculated by $-\log_{10}(I_S/I_0)$, where $I_S(\lambda)$ and $I_0(\lambda)$ are the transmission spectra through the sample with and without AuNP structures.

The transient absorption spectra ($\Delta A_i(\lambda)$, $i = A, B, C$) measured on samples A, B, and C are shown in Figures 3(a), (b), and (c), respectively, by the filled circles. In the TA measurements, 150 fs pulses at 800 nm were used as the pump and supercontinuum pulses extending from 340 to about 1000 nm were used as the probe. A pump fluence of about 400 μJ/cm^2 were employed for all of the TA measurements. The TA spectra in Figure 3 correspond to a delay of about $\Delta\tau = 1$ ps between the pump and probe pulses, where the signals reached their largest amplitudes.

The measured optical extinction spectra ($E_i(\lambda)$, $i = A, B, C$) are included in Figure 3 by the dotted curves, and the second-order differentials ($d^2E_i(\lambda)/d\lambda^2$) are plotted by the red curves. The red curves have been slightly rescaled and leveled to fit the measurement data of $\Delta A_i(\lambda)$. Clearly, although the TA data were measured on largely different samples, the spectra show quite similar features. All of these TA spectra are "peaked" at about 493 nm and "dipped" at about 550 nm, which have similar shapes and variations, implying physics not much dependent on the shapes, sizes, and distribution density of the gold nanostructures. The positive TA spectrum peaked at about 493 nm results from the "enhancement" of interband transition due to redshift of the threshold wavelength that was identified as a dip originally located at about 480 nm, as shown by all of the three spectra in Figure 2. The negative TA dipped at about 550 nm is attributed to the "quenching" of LSPR of the gold nanoparticles due the redshift of the threshold for interband transitions, where the original plasmonic electron oscillation is partially counteracted by interband electronic absorption. Therefore, such a neighbored "enhancement" and "quenching" behavior as an identity of the bandedge shift effects is verified convincingly by the measured TA spectrum.

Another important observation in Figure 3 is that the TA spectrum ($\Delta A_i(\lambda)$) fits perfectly the second-order differentials ($d^2E_i(\lambda)/d\lambda^2$) of the steady-state optical extinction spectra for all of the three samples. This is the most important experimental evidence for the photophysical mechanisms depicted in Figure 1. It needs to stress that the effects described here are different from the redshift of pure LSPR spectrum, which was a first-order differential of the optical extinction spectrum and has been applied in various plasmonic optical switches [18–23]. Thus, such a

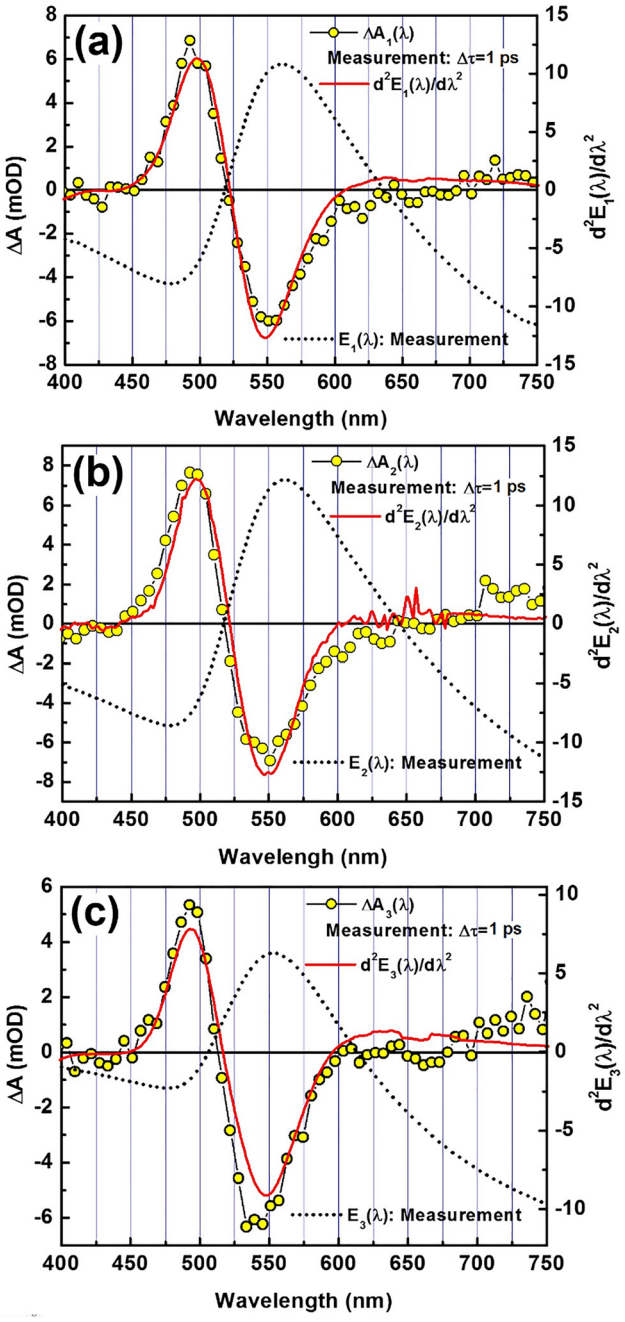

Figure 3: Measured transient absorption spectra (filled circles, ΔA) and calculated second-order differentials (solid red, $d^2E(\lambda)/d\lambda^2$) of the optical extinction spectra (dotted black, $E(\lambda)$) for samples A (a), B (b), and C (c), respectively.

second-order differentiation feature can be used not only as an identifier of the plasmonic quenching effect, but also as a discriminator between the bandedge shift and the pure plasmonic redshift effects in metallic structures. In Figure S1, we compare the calculated first- and second-order differentials of the measured optical extinction spectra for samples A, B, and C. Clearly, the second-order

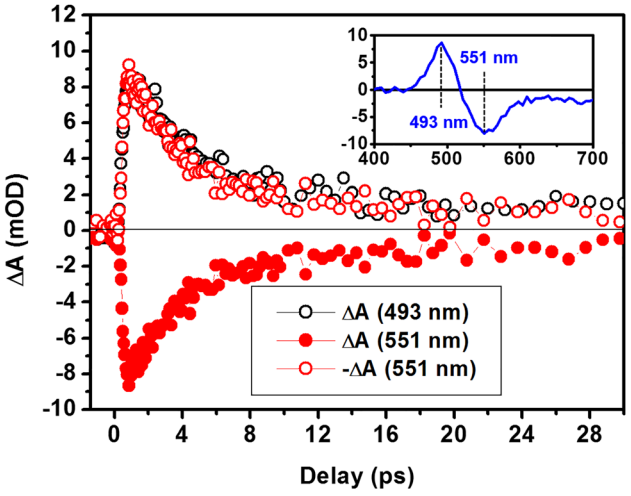

Figure 4: TA dynamics at 493 (empty black circles) and 551 nm (filled red circles), as well as the inversed TA dynamics at 551 nm (empty red circles) that is rescaled a bit to be normalized to that at 493 nm. Inset: TA spectrum at a delay of 1 ps.

differential curve is far different from the first-order, implying unique mechanism and solid identification evidence for the discovered photophysics.

Furthermore, since the enhanced interband transition and the quenched LSPR originated from the same mechanism of the redshifted threshold wavelength on the bandedge, these two processes should have a similar lifetime. Figure 4 shows the measured TA dynamics measured at 493 (ΔA(493 nm), open black circles) and 551 nm (ΔA(551 nm), filled red circles), which correspond exactly to the peak and dip features of the TA spectrum included in the inset, respectively. For clear comparison, a calculation of $-\Delta A$(551 nm) and a normalization of it to the peak intensity of ΔA(493 nm) is also included in Figure 4 by open red circles. Clearly, the transient absorption at 493 and 551 nm are varying in nearly the same dynamics with an equal lifetime. The revealed mechanisms are thus verified again.

As investigated in our previous work [24], optical heating by femtosecond laser pulses may induce thermal expansion of the lattices in gold. Enlargement of the lattice constant results in the shift of the Fermi level and lowering of the threshold for interband transitions. However, this effect is much weaker than the direct optical excitation-induced intraband transition. Nevertheless, this effect pushes bandedge-shift in the same direction as the intraband excitation, which also makes a small portion of contribution to the ultrafast optical performance.

It is understandable that the optical excitation induced bandedge shift is not limited to AuNPs, it is in nature a material-dependent mechanism, which applies also to gold films and even other metals. In Figure 5, we show the experimental results on a continuous gold film with a thickness of 130 nm. The black curve in Figure 5(a) is the steady-state optical extinction spectrum $E(\lambda)$, the blue and red curves are the first- and second-order differentials of the $E(\lambda)$, which read $dE(\lambda)/d\lambda$ and $d^2E(\lambda)/d\lambda^2$, respectively. The yellow-filled circles are the measured TA curve, which has been rescaled in amplitude to compare with $d^2E(\lambda)/d\lambda^2$. Perfect agreement between $\Delta A(\lambda)$ and $d^2E(\lambda)/d\lambda^2$ can be observed, which are both peaked at 498.3 nm, as highlighted by the red triangle. Thus, the disclosed mechanism is verified solidly again with the continuous gold film, showing generality of the identity mechanisms by the second-order differential.

Figure S2 summarizes the TA dynamics at different wavelengths within the spectral band from 469 to 592 nm. For a more detailed comparison, typical dynamic curves at 480.7, 498.3, and 515.9 nm are normalized and replotted in Figure 5(b). Consistent agreement between them can be observed and a lifetime of about 1.8 ps is resolved from the first-order exponential decay fitting, implying a common mechanism over the whole TA spectrum.

The TA spectrum is plotted more clearly in Figure S3(a), negative TA spectrum can be observed for wavelength longer than 555 nm, corresponding to the quenching of the plasmon band. Figure S3(b) plots the TA dynamics at 591.7 nm, which also shows a decay lifetime of about 1.8 ps, agreeing well with that in Figure 5(b). Clearly,

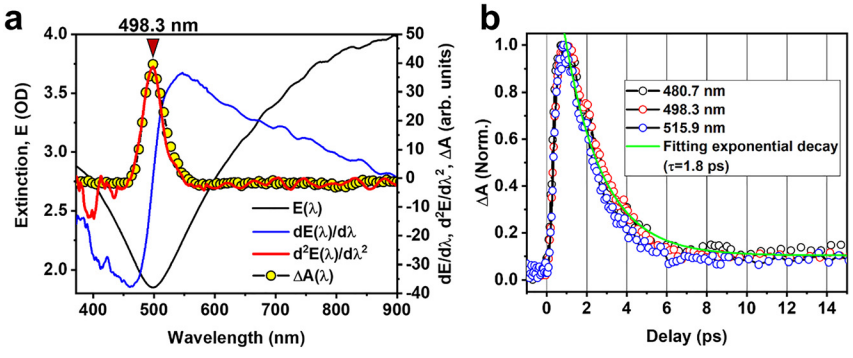

Figure 5: (a) Optical extinction (solid black) and TA (open circles) spectra measured on a gold film with a thickness of about 130 nm, and the calculated first- (sold blue) and second-order (solid red) differentials of the optical extinction spectrum, showing perfect agreement of ΔA with $d^2E/d\lambda^2$. (b) Normalized TA dynamics at 480.7, 498.3, and 515.9 nm.

the quenching effect is relatively weaker in the film than in the AuNPs. Thus, the bandedge redshift effect also exists with the gold film and can be confirmed as a general mechanism. In particular, the second-order differential behavior works again perfectly with different forms of metallic nanostructures. Such mechanisms apply to various metallic materials, plasmonic nanostructures, and plasmonic photophysical processes [25]. However, the discovered mechanism becomes explicitly observable when the excitation light intensity is high enough to enable strong intraband transitions and consequently transient depletion within the conduction band.

4 Conclusions

Extinguishment of localized surface plasmons is observed as an intrinsic optical performance in gold nanostructures under strong optical excitation by femtosecond laser pulses. Transient absorption spectroscopic experiments revealed the responsible mechanism as the transient depletion of the conduction band below the Fermi level due to strong intraband excitation. The resultant redshift of the bandedge enhances interband transitions and quenches the plasmonic optical extinction. The measured TA spectrum is observed as the second-order differential of the steady-state optical extinction spectrum, which can be used as the verification of the revealed photophysics and identity of the plasmonic quenching effect. This commonly existing photophysical process in the ultrafast optical response of metallic nanostructures should be taken into account in the design of functional plasmonic devices. It needs to be noted that the revealed mechanisms in the work are completely different from the generally observed optical-excitation-induced redshift of LSPR through enhanced electronic scattering.

Acknowledgments: The author acknowledges the National Natural Science Foundation of China (61735002, 12074020), the Beijing Municipal Education Commission (KZ202010005002), and the Beijing Key Lab of Microstructure and Property of Advanced Materials for the support.

Author contributions: All the authors have accepted responsibility for the entire content of this submitted manuscript and approved submission.

Research funding: None declared.

Conflict of interest statement: The author declares no conflicts of interest regarding this article.

References

[1] M. Perner, P. Bost, U. Lemmer, G. von Plessen, and J. Feldmann, "Optically induced damping of the surface plasmon resonance in gold colloids," *Phys. Rev. Lett.*, vol. 78, p. 2192, 1997.

[2] B. Lamprecht, A. Leitner, and F. R. Aussenegg, "SHG studies of plasmon dephasing in nanoparticles," *Appl. Phys. B*, vol. 68, p. 419, 1999.

[3] C. Fasolato, F. Sacchetti, P. Postorino, et al., "Ultrafast plasmon dynamics in crystalline LiF triggered by intense extreme UV pulses," *Phys. Rev. Lett.*, vol. 124, p. 184801, 2020.

[4] Y. H. Xian, Y. Cai, X. Y. Sun, et al., "Refractory plasmonic metal nitride nanoparticles for broadband near-infrared optical switches," *Laser Photonics Rev.*, vol. 13, p. 1900029, 2019.

[5] X. P. Zhang, B. Q. Sun, J. M. Hodgkiss, and R. H. Friend, "Tunable ultrafast optical switching via waveguided gold nanowires," *Adv. Mater.*, vol. 20, pp. 4455–4459, 2008.

[6] A. Krasnok, S. Li, S. Lepeshov, R. Savelev, D. G. Baranov, and A. Alu, "All-optical switching and unidirectional plasmon launching with nonlinear dielectric nanoantennas," *Phys. Rev. Appl.*, vol. 9, p. 14015, 2018.

[7] Y. G. Sang, X. J. Wu, S. S. Raja, et al., "Broadband multifunctional plasmonic logic gates," *Adv. Opt. Mater.*, vol. 6, p. 1701368, 2018.

[8] L. Gao, L. Chen, H. Wei, and H. X. Xu, "Lithographically fabricated gold nanowire waveguides for plasmonic routers and logic gates," *Nanoscale*, vol. 10, pp. 11923–11929, 2018.

[9] F. F. Wang, Z. B. Gong, X. Y. Hu, X. Y. Yang, H. Yang, and Q. H. Gong, "Nanoscale on-chip all-optical logic parity checker in integrated plasmonic circuits in optical communication range," *Sci. Rep.*, vol. 6, p. 24433, 2016.

[10] H. Wei, Z. X. Wang, X. R. Tian, M. Kall, and H. X. Xu, "Cascaded logic gates in nanophotonic plasmon networks," *Nat. Commun.*, vol. 2, p. 387, 2011.

[11] H. Q. Zhang, B. Abhiraman, Q. Zhang, et al., "Hybrid exciton–plasmon–polaritons in van der Waals semiconductor gratings," *Nat. Commun.*, vol. 11, p. 3553, 2020.

[12] P. Vasa, W. Wang, R. Pomraenke, et al., "Optical Stark effects in J-aggregate-metal hybrid nanostructures exhibiting a strong exciton-surface-plasmon-polariton interaction," *Phys. Rev. Lett.*, vol. 114, p. 036802, 2015.

[13] G. C. Li, Q. Zhang, S. A. Maier, and D. Y. Lei, "Plasmonic particle-on-film nanocavities: a versatile platform for plasmon-enhanced spectroscopy and photochemistry," *Nanophotonics*, vol. 7, pp. 1865–1889, 2018.

[14] J. Hohlfeld, S. S. Wellershoff, J. Gudde, U. Conrad, V. Jahnke, and E. Matthias, "Electron and lattice dynamics following optical excitation of metals," *Chem. Phys.*, vol. 251, p. 237, 2000.

[15] S. I. Kudryashov, A. A. Samokhvalov, S. N. Shelygina, and V. P. Veiko, "Tuning of localized plasmon resonance in colloidal gold nano-particles by ultrafast interband photoinjection of free carriers: superplasmonic states?" *Appl. Phys. Lett.*, vol. 115, p. 161903, 2019.

[16] P. J. Guo, R. D. Schaller, J. B. Ktterson, and R. P. H. Chang, "Ultrafast switching of tunable infrared plasmons in indium tin oxide nanorod arrays with large absolute amplitude," *Nat. Photonics*, vol. 10, p. 267, 2016.

[17] X. P. Zhang, C. Huang, M. Wang, P. Huang, X. He, and Z. Wei, "Transient localized surface plasmon induced by femtosecond

interband excitation in gold nanoparticles," *Sci. Rep.*, vol. 8, p. 10499, 2018.
[18] Y. H. Lin and X. P. Zhang, "Ultrafast multipolar plasmon for unidirectional optical switching in a hemisphere-nanoshell array," *Adv. Opt. Mater.*, vol. 5, p. 1661088, 2017.
[19] J. Y. Bigot, J. C. Merle, O. Cregut, and A. Daunois, "Electron dynamics in copper metallic nanoparticles probed with femtosecond optical pulses," *Phys. Rev. Lett.*, vol. 75, pp. 4702–4705, 1995.
[20] X. L. Wang, Y. Guillet, P. R. Selvakannan, H. Remita, and B. Palpant, "Broadband spectral signature of the ultrafast transient optical response of gold nanorods," *J. Phys. Chem. C*, vol. 119, pp. 7416–7427, 2015.
[21] J. Y. Bigot, V. Halte, J. C. Merle, and A. Daunois, "Electron dynamics in metallic nanoparticles," *Chem. Phys.*, vol. 251, p. 181, 2000.
[22] S. Link, C. Burda, Z. L. Wang, and M. A. El-Sayed, "Electron dynamics in gold and gold-silver alloy nanoparticles: the influence of a nonequilibrium electron distribution and the size dependence of the electron-phonon relaxation," *J. Chem. Phys.*, vol. 111, p. 1255, 1999.
[23] Y. Takeda, O. A. Plaksin, H. S. Wang, K. Konoi, N. Umeda, and N. Kishimoto, "Surface plasmon resonance of Au nanoparticles fabricated by negative ion implantation and grid structure toward plasmonic applications," *Opt. Rev.*, vol. 13, p. 231, 2006.
[24] X. P. Zhang, M. Wang, F. W. Tang, et al., "Transient electronic depletion and lattice expansion induced ultrafast bandedge plasmons," *Adv. Sci.*, vol. 7, p. 1902408, 2020.
[25] G. C. Li, Y. L. Zhang, J. Jiang, Y. Luo, and D. Y. Lei, "Metal-substrate-mediated plasmon hybridization in a nanoparticle dimer for photoluminescence line-width shrinking and intensity enhancement," *ACS Nano*, vol. 11, pp. 3067–3080, 2017.

Supplementary Material: The online version of this article offers supplementary material (https://doi.org/10.1515/nanoph-2020-0603).